Hydrogen Storage in Microporous Hypercrosslinked Organic Polymer Networks

ARTICLE *in* CHEMISTRY OF MATERIALS · APRIL 2007

Impact Factor: 8.35 · DOI: 10.1021/cm070356a

Hydrogen Storage in Microporous Hypercrosslinked Organic Polymer Networks

Colin D. Wood, Bien Tan, Abbie Trewin, Hongjun Niu, Darren Bradshaw, Matthew J. Rosseinsky, Yaroslav Z. Khimyak, Neil L. Campbell, Ralph Kirk, Ev Stöckel, and Andrew I. Cooper*

Department of Chemistry, The University of Liverpool, Crown Street, Liverpool L69 3BX, United Kingdom

Received February 5, 2007

A series of hypercrosslinked polymer networks has been synthesized by the self-condensation of bischloromethyl monomers such as dichloroxylene (DCX), 4,4′-bis(chloromethyl)-1,1′-biphenyl (BCMBP), and 9,10-bis(chloromethyl)anthracene (BCMA). These materials are predominantly microporous and exhibit Brunauer−Emmett−Teller (BET) surface areas of up to 1904 m^2/g as measured by N_2 adsorption at 77.3 K (Langmuir surface area = 2992 m^2/g). Networks based on BCMBP exhibit a gravimetric storage capacity of 3.68 wt % at 15 bar and 77.3 K, the highest yet reported for an organic polymer. The micro- and mesostructure of the networks is explained by a combination of solid-state NMR, gas sorption measurements, pycnometry, and molecular simulations. The isosteric heat of sorption for H_2 on these materials is found to be in the range 6−7.5 kJ/mol. A molecular model is presented for a *p*-DCX network that simulates well certain key physical properties such as pore volume, pore width, absolute density, and bulk density. This model also predicts the isotherm shape and isosteric heat for H_2 sorption at 77.3 and 87.2 K but overestimates the absolute degree of H_2 uptake, most likely because of a degree of occluded, inaccessible porosity in the real physical samples.

Introduction

The widespread use of hydrogen as a fuel is limited presently by the lack of a convenient, safe, and cost-effective method of H_2 storage.[1] A large number of materials have been investigated as physisorptive H_2 adsorbents, including polymers, carbon,[2−4] fullerenes and nanotubes,[5] zeolites,[4,6] and metal−organic frameworks (MOFs).[7−14] None of these materials meets the current criteria of size, recharge kinetics, cost, and safety required for use in transportation systems. The 2010 Department of Energy (DOE) gravimetric and volumetric storage targets for H_2 are 6.0 wt % and 45 g H_2/L, respectively. These targets are extremely challenging, particularly because they are system targets; that is, calculations of storage capacity should include pressure containment, valves, cooling systems, etc. As such, gravimetric capacities significantly greater than 6.0 wt % solely on the basis of the storage material would likely be required. The use of elevated pressures (and the necessary containment technology) or low temperatures (with the associated cooling systems) will generally increase system weights and exacerbate this problem. Moreover, there is an important distinction between storage capacity and delivery capacity, the latter of which is by definition lower.[15]

The storage of hydrogen in porous materials by physisorption is made difficult by the fundamentally weak interactions that exist between gas and sorbent at temperatures well above the critical temperature for H_2 (−240.17 °C). Substantial storage at moderate temperatures

* Corresponding author. E-mail: aicooper@liv.ac.uk.

(1) Schlapbach, L.; Züttel, A. *Nature* **2001**, *414*, 353.
(2) (a) Panella, B.; Hirscher, M.; Roth, S. *Carbon* **2005**, *43*, 2209. (b) Kowalczyk, P.; Bhatia, S. K. *J. Phys. Chem. B* **2006**, *110*, 23770. (c) Yushin, G.; Dash, R.; Jagiello, J.; Fischer, J. E.; Gogotsi, Y. *Adv. Funct. Mater.* **2006**, *16*, 2288. (d) Dillon, A. C.; Heben, M. J. *Appl. Phys. A: Mater. Sci. Process.* **2001**, *72*, 133. (d) Yang, Z. X.; Xia, Y. D.; Sun, X. Z.; Mokaya, R. *J. Phys. Chem. B* **2006**, *110*, 18424−18431.
(3) Zhao, X. B.; Xiao, B.; Fletcher, A. J.; Thomas, K. M. *J. Phys. Chem. B* **2005**, *109*, 8880.
(4) Chu, X. Z.; Zhou, Y. P.; Zhang, Y. Z.; Su, W.; Sun, Y.; Zhou, L. *J. Phys. Chem. B* **2006**, *110*, 22596.
(5) (a) Kim, Y. H.; Zhao, Y. F.; Williamson, A.; Heben, M. J.; Zhang, S. B. *Phys. Rev. Lett.* **2006**, *96*, 016102. (b) Deng, W. Q.; Xu, X.; Goddard, W. A. *Phys. Rev. Lett.* **2004**, *92*, 166103. (c) Züttel, A.; Sudan, P.; Mauron, P.; Kiyobayashi, T.; Emmenegger, C.; Schlapbach, L. *Int. J. Hydrogen Energy* **2002**, *27*, 203.
(6) Zecchina, A.; Bordiga, S.; Vitillo, J. G.; Ricchiardi, G.; Lamberti, C.; Spoto, G.; Bjorgen, M.; Lillerud, K. P. *J. Am. Chem. Soc.* **2005**, *127*, 6361.
(7) (a) Rosi, N. L.; Eckert, J.; Eddaoudi, M.; Vodak, D. T.; Kim, J.; O'Keeffe, M.; Yaghi, O. M. *Science* **2003**, *300*, 1127. (b) Chen, B. L.; Ockwig, N. W.; Millward, A. R.; Contreras, D. S.; Yaghi, O. M. *Angew. Chem., Int. Ed.* **2005**, *44*, 4745. (c) Rowsell, J. L. C.; Yaghi, O. M. *Angew. Chem., Int. Ed.* **2005**, *44*, 4670. (d) Fletcher, A. J.; Thomas, K. M.; Rosseinsky, M. J. *J. Solid. State Chem.* **2005**, *178*, 2491. (e) Frost, H.; Duren, T.; Snurr, R. Q. *J. Phys. Chem. B* **2006**, *110*, 9565. (f) Sun, D. F.; Ma, S. Q.; Ke, Y. X.; Collins, D. J.; Zhou, H. C. *J. Am. Chem. Soc.* **2006**, *128*, 3896.
(8) Wong-Foy, A. G.; Matzger, A. J.; Yaghi, O. M. *J. Am. Chem. Soc.* **2006**, *128*, 3494.
(9) Zhao, X. B.; Xiao, B.; Fletcher, A. J.; Thomas, K. M.; Bradshaw, D.; Rosseinsky, M. J. *Science* **2004**, *306*, 1012.
(10) Lin, X.; Jia, J. H.; Zhao, X. B.; Thomas, K. M.; Blake, A. J.; Walker, G. S.; Champness, N. R.; Hubbestey, P.; Schroder, M. *Angew. Chem., Int. Ed.* **2006**, *45*, 7358.
(11) Surblé, S.; Millange, F.; Serre, C.; Düren, T.; Latroche, M.; Bourrelly, S.; Llewellyn, P. L.; Férey, G. *J. Am. Chem. Soc.* **2006**, *128*, 14889.
(12) Ma, S. Q.; Zhou, H. C. *J. Am. Chem. Soc.* **2006**, *128*, 11734.
(13) Férey, G.; Mellot-Draznieks, C.; Serre, C.; Millange, F.; Dutour, J.; Surblé, S.; Margiolaki, I. *Science* **2005**, *309*, 2040.
(14) Férey, G.; Latroche, M.; Serre, C.; Millange, F.; Loiseau, T.; Percheron-Guegan, A. *Chem. Commun.* **2003**, 2976.
(15) Bhatia, S. K.; Myers, A. L. *Langmuir* **2006**, *22*, 1688.

10.1021/cm070356a CCC: $37.00
Published on Web 03/23/2007 PAGE EST: 14.1

is hard to achieve because the isosteric heat of adsorption for hydrogen on most carbonaceous materials is much too low (5−10 kJ mol^{-1}). For this reason, hydrogen physisorption has usually been investigated at 77.3 K, a temperature which is commensurate with isosteric heats of adsorption in this range.[15] The maintenance of such low temperatures and the associated system weight implications offer substantial practical challenges. This has prompted researchers to investigate, for example, "spillover" mechanisms[16] or MOFs that exhibit kinetic trapping behavior.[9] Even if low temperatures are employed, a generic challenge to physisorptive H_2 storage is the very high surface areas that are required in order to approach the DOE targets. For example, if one assumes 2D hexagonal close packing of Lennard−Jones dihydrogen on activated carbon, then the molecular area can be estimated as 0.0956 nm^2.[15] It follows that a maximum specific H_2 capacity of 3.47×10^{-5} g H_2/m^2 substrate would be obtainable and hence a physical surface area of 1729 m^2/g would be required to achieve the DOE gravimetric target of 6.0 wt % as the saturation pressure is approached. As pointed out by Bhatia and Myers,[15] "idealized" slit pore carbon has a calculated surface area in excess of this value (2630 m^2/g) but the maximum potential H_2 delivery (as opposed to storage) still falls short of the 6.0 wt % gravimetric target, even in this idealized case. It is therefore clear that extremely high internal physical surface areas are a prerequisite for H_2 storage by physisorption, at least in the absence of other potential mechanisms such as kinetic trapping.[9] This problem has been addressed most successfully via the use of MOF materials in which very high surfaces areas (greater than than 4000 m^2/g as calculated by N_2 sorption using the Langmuir model)[17] have been achieved. A major advantage is that the pore structure in MOFs can be fine-tuned in order to maximize H_2 storage density.[18] Recently, MOFs have exhibited storage capacities of more than 6.0 wt % H_2 on the basis of the material weight at 77.3 K at elevated pressures (20−90 bar).[8,10]

Porous organic polymers possess a number of potential advantages as sorbents for H_2 storage. First, polymers can be composed solely of light elements. Second, there exist a large number of synthetic routes by which a wide range of functionalities can be introduced, for example, moieties that could enhance H_2 binding affinities.[18] Third, polymers are a scalable technology and there are already examples of systems (e.g., macroporous polymer resins for separations) that are produced commercially on a large scale. A less obvious advantage is that porous organic polymers can be produced in a molded "monolithic" form.[19,20] This may avoid volumetric storage issues relating to the packing of porous particulate materials. A significant drawback is the very limited number of routes to produce predominantly microporous organic polymers with high specific surface areas (>1000 m^2/g). "Polymers of intrinsic microporosity" (PIMs)[21] are a class of microporous solids with surface areas in the range 500−1064 m^2/g, which results from their rigid and contorted molecular structures.[22−24] Recently, PIMs have been demonstrated to adsorb around 1.5−1.7 wt % H_2 at 77.3 K and 1 bar and up to 2.71 wt % at 10 bar.[23,24] Hypercrosslinked polymers represent another class of predominantly microporous organic materials that can exhibit high surface areas.[25−28] The permanent porosity in hypercrosslinked materials is a result of extensive chemical crosslinks that prevent the polymer chains from collapsing into a dense, nonporous state.[29] The most well-studied hypercrosslinked materials are "Davankov-type"[26] resins,[25−28] which are prepared by post-cross-linking of polystyrenic networks and can exhibit apparent BET surface areas as high as 2090 m^2/g.[30] We have shown recently in a brief communication that hypercrosslinked polystyrene (BET surface area = 1466 m^2/g) can reversibly adsorb up to 3.04 wt % H_2 at 77 K and 15 bar.[31] Germain et al. described similar low-pressure sorption properties for a hypercrosslinked polystyrene material[32] and much lower H_2 storage capacities for a range of commercially available macroporous polymer sorbents.

In this study, we describe an alternative route to producing microporous organic polymers based on the step growth polycondensation of dichloroxylene (DCX)[27] and other bischloromethyl monomers. We show that materials with very high surface areas (∼1900 m^2/g BET; ∼3000 m^2/g Langmuir) can be obtained by varying the structure of the monomer. The resulting materials can adsorb up to around 3.7 wt % H_2 at 77 K and 15 bar. We have used a combination of solid-state NMR, gas sorption measurements, and atomistic simulations to rationalize the surface area, pore size, and H_2 sorption properties of these polymers. We believe that this flexible methodology represents an important advance for the future design of purely organic sorbents with enhanced gas storage capacities and for a range of other applications.

(16) Li, Y. W.; Yang, R. T. *J. Am. Chem. Soc.* **2006**, *128*, 8136.
(17) Rowsell, J. L. C.; Yaghi, O. M. *J. Am. Chem. Soc.* **2006**, *128*, 1304.
(18) Lee, H.; Choi, W. I.; Ihm, J. *Phys. Rev. Lett.* **2006**, *97*, 056104.
(19) (a) Cooper, A. I.; Holmes, A. B. *Adv. Mater.* **1999**, *11*, 1270. (b) Hebb, A. K.; Senoo, K.; Bhat, R.; Cooper, A. I. *Chem. Mater.* **2003**, *15*, 2061.
(20) Svec, F.; Fréchet, J. M. J. *Science* **1996**, *273*, 205.
(21) Budd, P. M.; Ghanem, B. S.; Makhseed, S.; McKeown, N. B.; Msayib, K. J.; Tattershall, C. E. *Chem. Commun.* **2004**, 230.
(22) Budd, P. M.; McKeown, N. B.; Fritsch, D. *J. Mater. Chem.* **2005**, *15*, 1977.
(23) Ghanem, B. S.; Msayib, K. J.; McKeown, N. B.; Harris, K. D. M.; Pan, Z.; Budd, P. M.; Butler, A.; Selbie, J.; Book, D.; Walton, A. *Chem. Commun.* **2007**, 67.
(24) McKeown, N. B.; Gahnem, B.; Msayib, K. J.; Budd, P. M.; Tattershall, C. E.; Mahmood, K.; Tan, S.; Book, D.; Langmi, H. W.; Walton, A. *Angew. Chem., Int. Ed.* **2006**, *45*, 1804.
(25) (a) Davankov, V. A.; Tsyurupa, M. P. *React. Polym.* **1990**, *13*, 27. (b) Sidorov, S. N.; Bronstein, L. M.; Davankov, V. A.; Tsyurupa, M. P.; Solodovnikov, S. P.; Valetsky, P. M.; Wilder, E. A.; Spontak, R. J. *Chem. Mater.* **1999**, *11*, 3210.
(26) Davankov, V. A.; Rogozhin, S. V.; Tsyurupa, M. P. U.S. Patent 3 729 457, 1971.
(27) Tsyurupa, M. P.; Davankov, V. A. *React. Funct. Polym.* **2002**, *53*, 193.
(28) Tsyurupa, M. P.; Davankov, V. A. *React. Funct. Polym.* **2006**, *66*, 768.
(29) (a) Davankov, V. A.; Pastukhov, A. V.; Tsyurupa, M. P. *J. Polym. Sci., Part B: Polym. Phys.* **2000**, *38*, 1553. (b) Pastukhov, A. V.; Tsyurupa, M. P.; Davankov, V. A. *J. Polym. Sci., Part B: Polym. Phys.* **1999**, *37*, 2324.
(30) Ahn, J. H.; Jang, J. E.; Oh, C. G.; Ihm, S. K.; Cortez, J.; Sherrington, D. C. *Macromolecules* **2006**, *39*, 627.
(31) Lee, J. Y.; Wood, C. D.; Bradshaw, D.; Rosseinsky, M. J.; Cooper, A. I. *Chem. Commun.* **2006**, 2670.
(32) Germain, J.; Hradil, J.; Fréchet, J. M. J.; Svec, F. *Chem. Mater.* **2006**, *18*, 4430.

Experimental Section

Chemicals. Vinylbenzyl chloride (VBC, Aldrich, 30:70 w/w mixture of *p*-VBC and *m*-VBC isomers), divinylbenzene (DVB, Aldrich, 80% grade), poly(vinyl alcohol) (PVA 88% hydrolyzed, M_w = 31 000−50 000 g/mol), dichloroxylene (*o*-, *m*-, *p*-DCX, Aldrich, >98%), 4,4′-bis(chloromethyl)-1,1′-biphenyl (BCMBP, Aldrich, 95%), and bis(chloromethyl) anthracene (BCMA, ABCR GmbH & Co., 95%) were all used as received. 2,2′-Azobis-(isobutyronitrile) (AIBN, Fisher) was recrystallized from methanol prior to drying under reduced pressure.

Synthesis of Hypercrosslinked Polymers. *(a) HCPVBC "Davankov Resins".*[31] (i) Synthesis of gel-type precursor: The gel-type precursor resin was obtained by free radical suspension polymerization. The monomer phase consisted of vinylbenzyl chloride (VBC, Aldrich, 30:70 w/w mixture of *p*-VBC and *m*-VBC isomers, 98 wt %, 39.10 g), divinylbenzene (DVB, Aldrich, 80% grade, 2 wt %, 0.80 g), and 2,2′-azobis(isobutyronitrile) (AIBN, 0.5 wt % based on monomers). The aqueous phase consisted of distilled water (500 cm^3), poly(vinyl alcohol) (3.75 g, 88% hydrolyzed, M_w = 31 000−50 000 g/mol) and sodium chloride (16.5 g). The organic phase was suspended in the aqueous phase at 80 °C by stirring at 425 rpm under N_2 using a rotary impeller. After 6 h, the beads were filtered; washed three times with water, methanol, and diethyl ether; and dried under reduced pressure for 24 h at 50 °C. (ii) Hypercrosslinking reaction: The DVB−VBC gel-type precursor resin (2.5 g) was swollen in 1,2-dichloroethane (DCE, 40 cm^3) under N_2 for 3 h. Ferric chloride ($FeCl_3$, 2.61 g) in DCE (40 cm^3) was added to the solution, which was then heated at 80 °C for 18 h. Alternatively, the reaction was heated to 100 °C for 1 h using a microwave-accelerated reaction system (CEM corp USA) at 1200 W. The resulting hypercrosslinked beads were filtered and washed three times with water, methanol, and diethyl ether followed by drying for 24 h at 50 °C. Elemental analysis (HCPVBC resin, 1657 m^2/g): C, 87.01; H, 6.34; Cl, 3.54.

(b) Polycondensation of Bis(chloromethyl) Monomers (DCX, BCMBP, or BCMA). To a solution of monomer(s) in anhydrous dichloroethane (DCE, 10 mL), a DCE solution of $FeCl_3$ was added under nitrogen. The resulting mixture was heated using either standard thermal heating (samples **28**−**49**) or a microwave reactor (Explorer or MARS systems; CEM corporation, USA, samples **1**−**27**) while stirring at 100 or 80 °C, respectively. The resulting brown precipitate was washed once with water, three times with methanol (until the filtrate was clear), and with diethyl ether followed by drying for 24 h at 60 °C. Typical elemental anal. For **27**: C, 81.96; H, 5.38; Cl, 5.24. For **43**: C, 87.24; H, 5.16; Cl, 5.00. ***Caution****: Friedel−Crafts chemistry can be strongly exothermic and can lead to rapid temperature ramps. These reactions can generate very substantial pressure if carried out in sealed microwave tubes; this should be done only in suitably pressure-rated apparatus equipped with pressure sensors and appropriate safety release mechanisms.*

Sorption Isotherms: Surface Areas, Pore Sizes and H_2 Uptakes. The dry state polymer surface areas and pore size distributions were measured using either a Micromeritics ASAP 2420 or ASAP 2020 adsorption analyzer. Samples were degassed for 10 h at 110 °C before analysis. Apparent surface areas were measured using either the Brunauer−Emmett−Teller (BET) or Langmuir method at 77.3 K. We also assessed the apparent surface area by application of the Langmuir equation to the hydrogen adsorption isotherms measured at 77.3 K over the pressure range 0.15−1.13 bar. This may avoid problems associated the overestimation of surface areas as a result of condensation of N_2 in micropores.[32] Hydrogen adsorption isotherms were measured volumetrically up to 1.13 bar (Micromertics 2420) or gravimetrically (see below).[31]

Helium Pycnometry. It is challenging to accurately measure the true (or "absolute") density for microporous materials of this type. The technique of helium pycnometry is problematic because of the difficulties involved in adequately purging high-surface-area sorbents in the pycnometer.[31] We overcame this by loading the sample after thorough degassing while still hot and allowing the sample to cool in the pycnometer under a flow of helium.[33] In this way, we achieved good reproducibility for the true density measurement.

Gravimetric Sorption Measurements. The gravimetric hydrogen sorption studies were carried out using a Hiden Isochema (Warrington, U. K.) Intelligent Gravimetric Analyzer (IGA) equipped with a microgram balance and 2, 100, and 20 000 mbar barotron pressure transducers. Temperature control was via a furnace for desolvation of the porous polymeric materials and by immersion of the reaction chamber into liquid nitrogen contained in a cryogenic vessel during isotherm measurement. Samples were placed into a stainless steel mesh bucket and covered with a small amount of quartz wool to prevent sample displacement from the holder when gas was admitted into the chamber. All samples were activated by outgassing at 150 °C under a high dynamic vacuum (1×10^{-7} mbar) until a constant mass had been reached; typically overnight. Mass losses for the samples tested were in the range 1.5−3.6%. Hydrogen gas of purity 99.9995% (N5.5, research grade) supplied by BOC gases was used for this study. All admittance pipe work was thoroughly decontaminated under a high dynamic vacuum prior to the admission of any gas, and the gas was passed though a coil of total length 3 m immersed in liquid nitrogen. An activated carbon standard of known surface area and hydrogen sorption properties was used to validate all measurement protocols. All isotherm data points were fitted by the IGASwin systems software v.1.03.84 (Hiden Isochema 2002) using a linear driving force model, and all data were corrected for buoyancy effects using the density of the materials determined from helium pycnometry measurements.

Isosteric Heats of Sorption. Heats of adsorption were determined from hydrogen adsorption isotherms up to a pressure of 1.13 bar at both liquid nitrogen (77.3 K) and argon (87.2 K) temperatures using a Micromeritics ASAP 2420 instrument and the standard calculation routines in the Datamaster offline data reduction software (Micromeritics).

Solid-State NMR. Solid-state NMR spectra were measured on a Bruker Avance 400 DSX spectrometer operating at 100.61 MHz for ^{13}C and 400.13 MHz for ^1H. $^1H-^{13}C$ cross polarization magic angle spinning (CP/MAS) NMR experiments were carried out at MAS of 8.0 kHz using zirconia rotors 4 mm in diameter. TOSS pulse sequence was used for the acquisition.[34] The ^1H $\pi/2$ pulse was 3.3 μs and TPPM decoupling[35] was used during the acquisition. The Hartmann−Hahn condition was set using hexamethylbenzene. The spectra were measured using a contact time of 2.0 ms and relaxation delay of 5.0 s. Typically, 1024 scans were accumulated. The $^{13}C\{^1H\}$ MAS NMR spectra were measured at a MAS rate of 8 kHz using TPPM decoupling. The ^{13}C $\pi/2$ pulse was 3.5 μs. The spectra were measured using a recycle delay of 15.0 s. Typically, 1024 scans were accumulated. The values of chemical shift are referred to TMS. The analysis of the spectra (deconvolution and integration) was carried out using Bruker TOPSPIN software.

(33) Mauguet, M. C.; Montillet, A.; Comiti, J. *J. Mater. Sci.* **2005**, *40*, 747.
(34) Schmidt-Rohr, K.; Spiess, H. W. *Multidimensional Solid-State NMR and Polymers*; Academic Press: London, 1994.
(35) Bennett, A. E.; Rienstra, C. M.; Auger, M.; Lakshmi, K. V.; Griffin, R. G. *J. Chem. Phys.* **1995**, *103*, 6951.

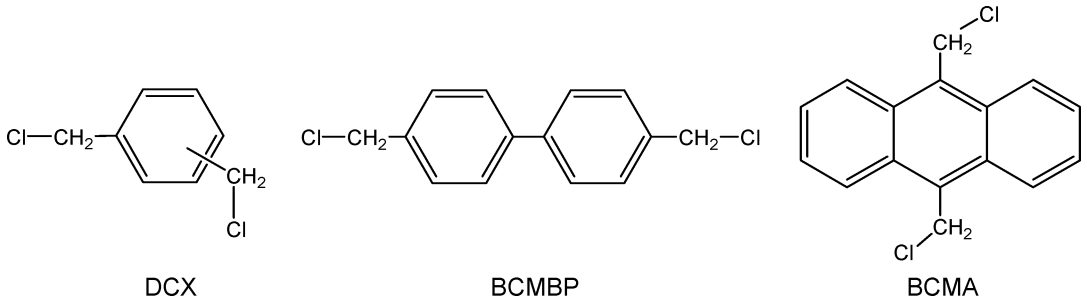

Figure 1. Monomers used for the synthesis of the hypercrosslinked polymer networks. DCX: Dichloroxylene (ortho-, meta-, and para-isomers). BCMBP: 4,4′-Bis(chloromethyl)-1,1′-biphenyl. BCMA: Bis(chloromethyl)anthracene.

Atomistic Simulations and DFT Calculations. Molecular models for polymer networks were generated using the Materials Studio Modeling 4.0 package (Accelrys Inc., San Diego, CA, 2005). The Polymer Building tool was used to construct the networks and the models were fully relaxed using the Discover molecular mechanics and dynamics simulation module with the COMPASS forcefield.[36] The Amorphous Cell module was used to combine these fragments with periodic boundary conditions applied. Hydrogen sorption isotherms were calculated using the Sorption module within Materials Studio. The Universal forcefield was used at a medium-quality calculation level. DFT calculations were performed using the VASP computer code with the standard set of ultra-soft pseudopotentials supplied. Exchange and correlatin were treated with the PW91 GGA approximation. The Brillouin zone was sampled via a $3 \times 3 \times 3$ Monkhorst−Pack k-point mesh, with a plane wave cutoff energy of 340 eV.

Results and Discussion

Dichloroxylene (DCX) Networks. The Friedel−Crafts-catalyzed self-condensation of *p*-dichloroxylene (*p*-DCX) was first described by Tsyurupa and Davankov.[27] It was reported that materials with BET surface areas of 900−1000 m^2/g could be obtained by using $SnCl_4$ as the catalyst and that these materials were swellable in toluene, methanol, and heptane.[27] No other characterization data was provided apart from BET surface areas in this brief report. We have explored the use of *p*-DCX, *m*-DCX, and *o*-DCX (Figure 1) as self-condensing monomers for the preparation of high-surface-area polymer networks for H_2 storage (Table 1). Anhydrous iron trichloride ($FeCl_3$) was used throughout as the Friedel−Crafts catalyst because it shows good activity for the preparation of hypercrosslinked polymers from poly(vinyl benzylchloride) (PVBC) precursors.[30,31] A wide range of reaction conditions was explored (Table 1, **1**−**24**) in order to identify materials with optimized pore structures and H_2 sorption properties. Overall, materials with BET surface areas in the range 600−1400 m^2/g were obtained using microwave heating to complete the polycondensation reaction (**1**−**24**). We evaluated the neat *p*-, *m*-, and *o*- isomers of DCX as well as mixtures of these isomers with the aim of identifying compositions with optimized pore size distributions that maximize H_2 sorption properties. A number of basic trends were identified. The incorporation of *o*-DCX was consistently detrimental to the generation of surface area in these materials, both when used individually or in mixtures with the *p*- and *m*- isomers. This is associated with the lower degree of condensation (i.e., crosslinking) achieved with *o*-DCX, as determined by solid-state NMR (see below). In general, both *m*-DCX and *p*-DCX gave rise to materials with quite similar BET surface areas under comparable reaction conditions. There was no clear evidence for any "synergistic" monomer compositions that produced materials with significantly higher surface areas than the respective *m*-DCX and *p*-DCX homopolymers. As might be expected, the surface area in the materials increased with increasing reaction time, up to a maximum after 60 min (**25**−**27**), presumably because the crosslinking density was maximized at this point. Increasing the monomer concentration much above 6−7.5% w/v (**28**−**33**) slightly decreased the surface area in the resulting materials, although this effect was small, quite in contrast to macroporous polymer monoliths based on vinyl monomers where the surface area may be very sensitive to monomer concentration.[19,20] Last, it was shown that the optimum $FeCl_3$ ratio was in the range 0.5−2 mol/mol based on the monomers (**35**−**41**). Catalyst ratios below this range led to decreased yields and surface areas, whereas much higher catalyst concentrations were detrimental to surface area in the resulting polymers. Studies on the reproducibility of the reaction (i.e., repeat reactions under the same conditions; **21**−**24**) showed some variation in both yield and surface area, possibly because of the propensity for these exothermic reactions to form "hot spots" and the general difficulty in controlling this on a small test scale (<2 g solids). By contrast, the reproducibility of the gas sorption measurements was found to be excellent (±3%); as such, we are confident that the variation in the materials properties for **21**−**24** arises from small variations in the reaction conditions and not from measurement variability. The highest BET surface area obtained for the DCX materials was 1431 m^2/g (**6**, *p*-DCX homopolymer); the equivalent Langmuir surface area (calculated by N_2 sorption) was 2281 m^2/g.

^{1}H−^{13}C CP/MAS NMR for DCX Networks. Solid-state NMR was used to investigate the molecular structure of these DCX networks. Figure 2 shows a series of ^{1}H−^{13}C CP/MAS NMR spectra for materials **4**−**6** as synthesized from *o*-DCX, *m*-DCX, and *p*-DCX, respectively. All spectra show three main peaks at ca. 35.9, 130.0, and 137.1 ppm. These can be assigned by comparison with literature on hypercrosslinked polystyrene[37] as arising from the methylene linkers in the material (35.9 ppm), the non-substituted (i.e., hydrogen-

(36) Sun, H. *J. Phys. Chem. B* **1998**, *102*, 7338.

(37) Law, R. V.; Sherrington, D. C.; Snape, C. E.; Ando, I.; Kurosu, H. *Macromolecules* **1996**, *29*, 6284.

Table 1. Synthesis Conditions, Surface Areas, and Gravimetric H_2 Uptakes for Hypercrosslinked Polymers[a]

	monomer (w/v %)	$FeCl_3$ (mol)[b]	*t* (min)[c]	*o*-DCX (mol)[d]	*m*-DCX (mol)[d]	*p*-DCX (mol)[d]	BCMBP	BCMA	yield (%)[e]	BET SA (m^2/g)[f]	Langmuir SA (N_2) (m^2/g)	Langmuir SA (H_2) (m^2/g)[g]	H_2 uptake (1.13 bar/77.3K) (wt %)[h]
1	2.5	1	60	1	0	0			30	600	924	498	0.89
2	2.5	1	60	0	1	0			59	1097	1707	806	1.37
3	2.5	1	60	0	0	1			60	1045	1608	798	1.35
4	12.5	1	60	1	0	0			59	896	1393	781	1.37
5	12.5	1	60	0	1	0			64	1377	2196	969	1.61
6	12.5	1	60	0	0	1			63	1431	2281	999	1.66
7	2.5	3	60	1	0	0			55	777	1200	675	1.19
8	2.5	3	60	0	1	0			60	1098	1716	925	1.59
9	2.5	3	60	0	0	1			66	963	1455	801	1.38
10	2.5	3	60	0	0.5	0.5			63	1131	1764	878	1.50
11	12.5	3	60	1	0	0			64	750	1142	659	1.18
12	12.5	3	60	0	1	0			74	1279	2026	832	1.41
13	12.5	3	60	0	0	1			70	1172	1788	832	1.42
14	12.5	3	60	0	0.5	0.5			60	1220	1946	827	1.40
15	2.5	2	60	0	0	1			61	1182	1820	824	1.41
16	2.5	2	60	0.5	0.5	0			58	1317	2020	873	1.48
17	12.5	2	60	0.5	0	0.5			62	1177	1903	811	1.39
18	7.5	1	60	0	0.5	0.5			48	1313	2022	853	1.44
19	7.5	3	60	0	1	0			72	1209	1884	842	1.42
20	7.5	3	60	0.5	0	0.5			68	1069	1636	795	1.36
21	7.5	2	60	0.33	0.33	0.33			65	1347	2068	930	1.56
22	7.5	2	60	0.33	0.33	0.33			34	1032	1596	827	1.42
23	7.5	2	60	0.33	0.33	0.33			63	1137	1832	773	1.32
24	7.5	2	60	0.33	0.33	0.33			65	1058	1670	769	1.30
25	4.0	1	20	0	0	1			57	1199	1881	879	1.47
26	4.0	1	40	0	0	1			63	1324	2027	998	1.67
27	4.0	1	60	0	0	1			62	1370	2096	1013	1.69 (3.18)
28	6.25	1	1080	0	0	1			63	1197	1833	924	1.56
29	12.5	1	1080	0	0	1			64	816	1260	655	1.14
30	25	1	1080	0	0	1			64	930	1300	708	1.23
31	50	1	1080	0	0	1			66	826	1157	616	1.06
32	100	1	1080	0	0	1			69	890	1360	882	1.52
33	160	1	1080	0	0	1			67	815	1274	738	1.29
35	3.75	0.05	1080	0	0	1			26	1062	1635	643	1.10
36	3.75	0.1	1080	0	0	1			35	1052	1621	651	1.10
37	3.75	0.2	1080	0	0	1			48	1169	1797	773	1.30
38	3.75	0.5	1080	0	0	1			60	1379	2128	933	1.56
39	3.75	1	1080	0	0	1			64	1391	2131	948	1.58
40	3.75	2	1080	0	0	1			65	1365	2098	932	1.56
41	3.75	3	1080	0	0	1			73	1215	1860	844	1.42
42	10.70[i]	1	1080			0	100		74	1874	2957	1002	1.56
43	9.93[i]	1	1080			25	75		70	1904	2992	1033	1.61 (3.68)
44	9.07[i]	1	1080			50	50		71	1786	2756	1035	1.62
45	8.31[i]	1	1080			75	25		67	1612	2476	1014	1.63
46	11.80[i]	1	1080			0		100	55	921	1402	808	1.41
47	10.70[i]	1	1080			25		75	52	1069	1620	870	1.48
48	9.65[i]	1	1080			50		50	43	1057	1616	852	1.43
49	8.52[i]	1	1080			75		25	55	1262	1933	856	1.44

[a] DCX = Dichloroxylene; BCMBP = 4,4′-bis(chloromethyl)-1,1′-biphenyl; BCMA = bis(chloromethyl)anthracene. [b] Molar ratio with respect to monomer; reaction solvent was 1,2-dichloroethane in all cases. [c] Samples **1**−**27** were polymerized using microwave heating (100 °C) and samples **28**−**49** using conventional heating (80 °C). [d] Molar ratio with respect to other monomers. [e] Determined gravimetrically after washing and drying. [f] Five-point BET values. [g] Calculated over the H_2 pressure range 0.15−1.13 bar. [h] Determined volumetrically using a Micromeritics 2420 analyzer. Figures in parentheses determined gravimetrically at 15 bar using a Hiden Isochema Intelligent Gravimetric Analyzer. [i] Concentrations calculated on a relative molar basis for the comonomers and catalyst, hence small variations in w/v % monomer concentrations.

bearing) aromatic carbons (130.0 ppm), and the substituted aromatic carbons (137.1 ppm), respectively. The minor resonance at ca. 42.1 ppm is attributable to the CH_2Cl groups. Such resonances are additionally broadened because of the $^{13}C-^{35,37}Cl$ residual dipolar coupling, which is not completely averaged out under MAS.[38] From peak intensities, it is possible to define a ratio, S/NS, to describe the ratio of the substituted and non-substituted aromatic carbons in the structure. One should be aware that the $^1H-^{13}C$ CP/MAS NMR spectra, in general, are not quantitative as the efficiency of CP depends on the strength of $^1H-^{13}C$ dipolar couplings defined by the $^1H-^{13}C$ distances and mobility of a particular functional group.[39] While preliminary studies of the $^1H-^{13}C$ CP/MAS kinetics for polymers **3** and **4** revealed faster CP kinetics for the non-substituted aromatic peaks, maximum intensity for both aromatic resonances was achieved after 1.0−1.5 ms contact time. Moreover, both resonances showed very similar ^1H relaxation times in the rotating frame.[39] The S/NS ratio was therefore determined from $^1H-^{13}C$ CP/MAS NMR spectra measured at contact time of 2.0 ms and can be considered at least semiquantitave. It is also important to note that the S/NS ratios derived from the $^1H-^{13}C$ CP/MAS NMR spectra are in good agreement with the values

(38) Thomas, B.; Paasch, S.; Steurnagel, S.; Eichele, K. *Solid State Nucl. Magn. Res.* **2001**, *20*, 108.

(39) Kolodziejski, W.; Klinowski, J. *Chem. Rev.* **2002**, *102*, 613−628.

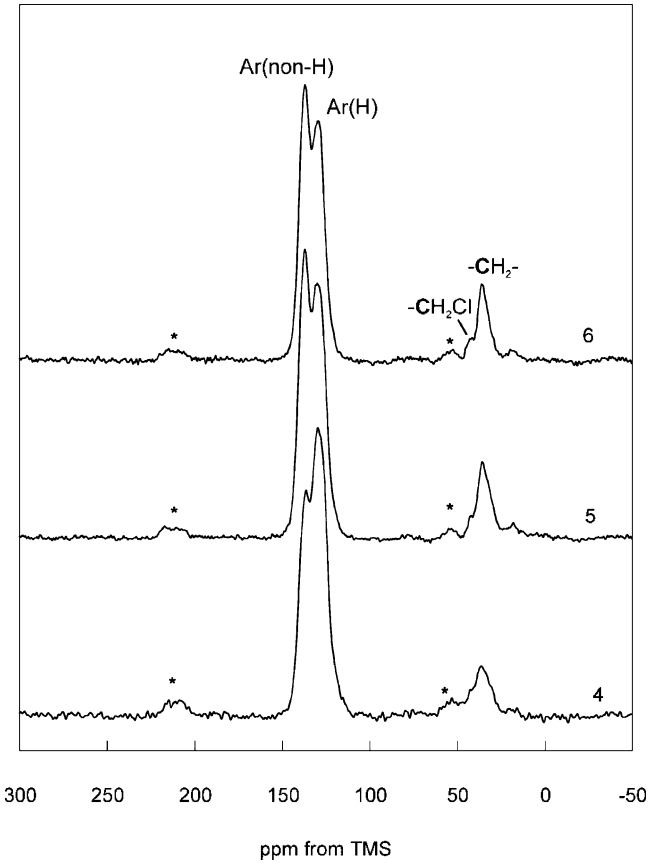

Figure 2. $^{1}H-^{13}C$ CP/MAS NMR spectra of porous polymers **4**−**6** (MAS rate 8 kHz, contact time 2.0 ms). Signals marked * can be assigned to spinning side bands.

determined from the $^{13}C\{^{1}H\}$ MAS NMR spectra (data not shown). For **5** and **6**, S/NS was determined to be 1.14 and 1.15, respectively. This is consistent with a condensed network where, on average, the number of substituted aromatic carbons is slightly greater than the number of non-substituted carbons; that is, a highly condensed network structure. By contrast, S/NS for **4** was found to be 0.78; a S/NS value of less than 1 indicates a polymer where there are fewer substituted aromatic carbons than non-substituted aromatic carbons. This implies a much less highly condensed network, and we suggest that it is this reduced level of crosslinking (and hence reduced network rigidity) that leads to the lower surface areas observed for samples derived from *o*-DCX. It is likely that *o*-DCX is prevented from realizing a more fully condensed network for steric reasons. An S/NS ratio of precisely 1 would indicate a network where, on average, one new carbon bond is made to each aromatic ring in order to achieve an equal number of substituted and unsubstituted aromatic carbons. This situation could arise (Figure 3a) in a hypothetical "infinite network" in which the contribution to the S/NS ratio of any monoreacted chloromethyl-bearing monomer units at the surface periphery of the molecule is ignored. In reality, this simple description cannot account for the properties of these materials; CH_2-Cl resonances are observed in the NMR and elemental analysis for *m*-DCX and *p*-DCX polymers showed residual chlorine contents of around 5% that can be ascribed to unreacted chloromethyl functionalities.[37] Moreover, it would be expected that the surface to volume ratio for these network materials would be rather high − they are microporous − and therefore that the contribution of monoreacted chloromethyl-bearing monomer units at the polymer surface might be significant. Because any monoreacted chloromethyl-bearing monomer units would contribute S/NS = 0.5 to the overall ratio (for example, the bottom left unit in Figure 3b), it would therefore be necessary that a significant number of aromatic units bear more than three substituents in order to achieve an average S/NS ratio greater than 1. This can be achieved in a variety of ways; for example, by the formation of double methylene bridges (Figure 3b),[37] by multiple Friedel−Crafts substitution reactions on individual aromatic rings, or by internal cyclization reactions within the network, each of which will increase the S/NS ratio. It is therefore likely that the molecular structure of these polymers is much more complex than the idealized scheme presented in Figure 3a, although the elucidation of such fine structural details for amorphous networks of this type represents a major analytical challenge.

4,4′-Bis(chloromethyl)-1,1′-biphenyl (BCMBP) Networks. In general, the incorporation of rigid moieties into network structures is beneficial for the generation of permanent microporosity both in polymers[21−31] and in MOFs.[7−14] We therefore investigated an "extended" variant of DCX 4,4′-bis(chloromethyl)-1,1′-biphenyl (BCMBP; Figure 1), as a monomer for microporous network formation. Both homopolymer networks of BCMBP (**42**) and copolymer networks with *p*-DCX (**43**−**45**) were produced. Polymer networks based on BCMP had significantly higher BET surface areas than any of the materials (**1**−**41**) synthesized using the three isomers of DCX. The BET surface area for **42** (produced from 100% BCMBP) was determined to be 1874 m^2/g (Langmuir surface area (N_2) = 2957 m^2/g); that is, more than 400 m^2/g higher than the most porous DCX-based networks. Interestingly, this effect was observed in systems in which BCMBP was the minority component; for example, **45** exhibited a BET surface area of 1612 m^2/g even though just 25% mol/mol BCMBP was used with respect to *p*-DCX (75% mol/mol). BCMBP "builds in" a rigid para geometry between neighboring aryl rings and it is likely that this enhances the degree of accessible porosity. This illustrates the prime importance of monomer design: whereas reaction conditions clearly exert an influence (samples **1**−**41**), all of the BCMBP-containing networks (**43**−**45**) had higher BET surface areas than the most porous DCX-based samples.

9,10-Bis(chloromethyl)anthracene (BCMA) Networks. By contrast, a structurally related rigid fused-ring monomer, BCMA (Figure 1a), did not lead to enhanced BET surface areas. The homopolymer of BCMA, **46**, exhibited a BET surface area (921 m^2/g) that was lower than observed for most of the DCX networks (**1**−**41**). Copolymers with *p*-DCX (**47**−**49**) exhibited higher BET surfaces areas with the largest surface area being observed for the minimum BCMA incorporation (**49**, 1262 m^2/g). It may be that the structure of BCMA is akin to ortho substitution on either side of a *p*-DCX monomer and that similar steric effects come into play as invoked for *o*-DCX, above. These data further highlight the fact that relatively small changes to monomer

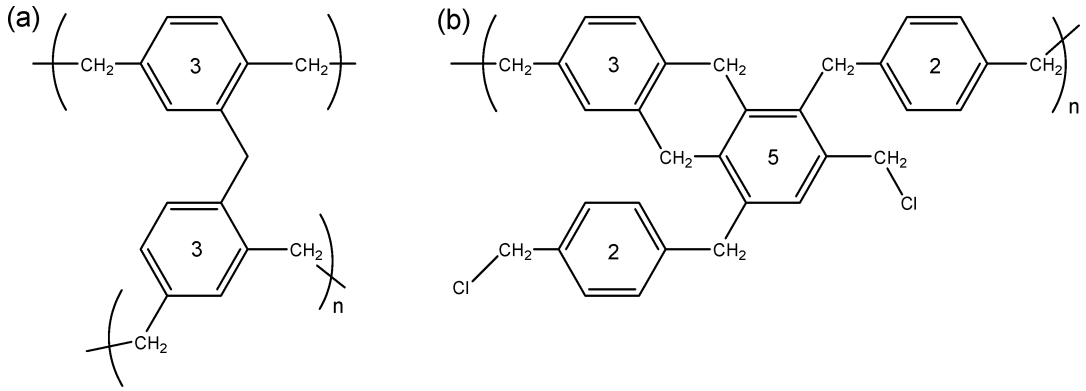

Figure 3. (a) Hypothetical idealized *p*-DCX network structure, which is consistent with a $^{1}H-^{13}C$ CP/MAS NMR ratio of substituted to non-substituted aromatic carbons (S/NS) of 1. Each aromatic unit bears precisely three substituents (as denoted by the numerals) if the peripheral terminal units are ignored (i.e., an "infinite" network is assumed). (b) Hypothetical fragment of a real *p*-DCX network, which is also consistent with S/NS = 1 and an average aromatic functionality of 3. This fragment contains both a double methylene bridge (which increases the average value of S/NS) and a monoreacted terminal chloromethyl unit (which decreases the average S/NS ratio).

structure can lead to large differences in the porous properties of the resulting materials.

Gas Sorption Properties. A primary aim of this study was to identify polymers with enhanced gravimetric H_2 storage properties. All samples (**1**−**49**) were characterized with respect to BET and Langmuir surface areas using N_2 as the sorbate molecule (Table 1). In addition, the H_2 sorption isotherm was measured volumetrically for every sample up to a pressure of 1.13 bar at 77.3 K. Figure 4a shows a plot of the maximum H_2 uptake observed (77.3 K, 1.13 bar) versus the apparent BET surface area for samples **1**−**49**. In general, the H_2 sorption was found to increase with apparent BET surface area, although the correlation was weak (Figure 4a). In fact, these data show that apparent BET surface area is quite a poor descriptor for the H_2 sorption properties for **1**−**49**. For example, it was found that polymers with very similar BET surface areas (e.g., **8** and **35**) exhibited maximum H_2 sorption values which differed by 50% or more. Similarly, samples could be identified with apparent BET surface areas that differed by more than 800 m^2/g and yet which gave rise to very similar maximum H_2 uptakes (e.g., **8** and **43**). An even more exaggerated trend was observed when the maximum H_2 uptake was plotted against the Langmuir surface area as calculated from N_2 sorption data (see the Supporting Information, Figure S1). Other authors have noted in studies involving activated carbons[40] that BET surface areas do not correlate very well with H_2 uptake and that micropore volume, for example, may be a better descriptor. The BET method is known to give rise to inflated surface areas for materials that are substantially microporous;[41] for an array of samples with varying pore size distributions (see below), this effect might well be expected to cause the scatter observed in Figure 4a. Moreover, as pointed out by Germain et al.,[32] it has been suggested[28] that hypercrosslinked polymers may swell in liquid nitrogen; again, any swelling would be expected to depend strongly on the physical level of crosslinking in the sample, thus introducing a further potential source of variability. A possible solution here is to evaluate surface areas using gases in the supercritical state[42] and to use monolayer-based

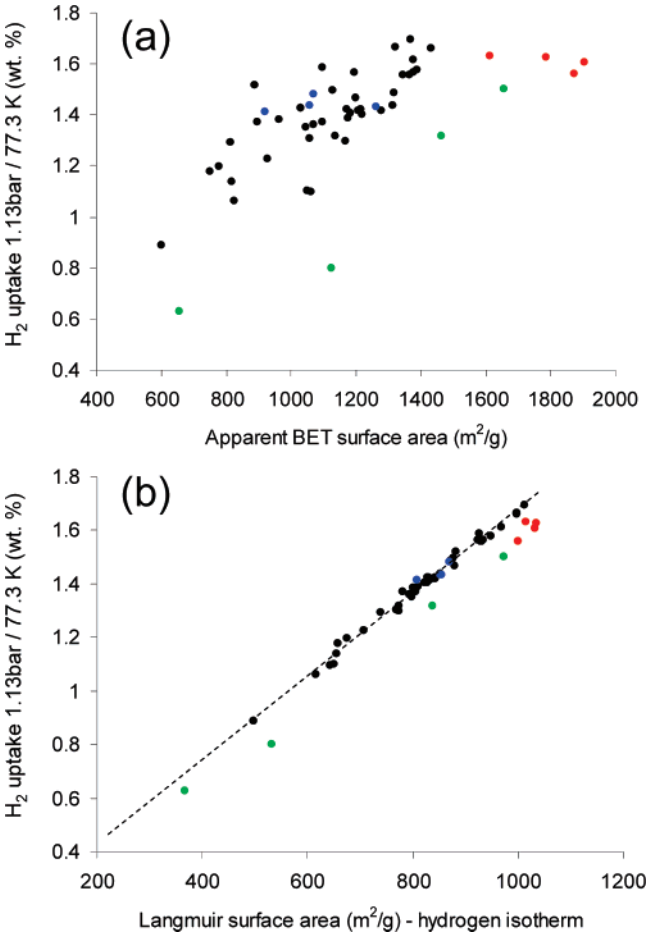

Figure 4. (a) Hydrogen uptake at 1.13 bar/77.3 K as a function of apparent BET surface area for a series of hypercrosslinked polymers: dichloro(xylene) (DCX) networks, **1**−**41** (black symbols); bis(chloromethyl)biphenyl (BCMBP) networks, **42**−**45** (red symbols); bis(chloromethyl)anthracene (BCMA) networks, **46**−**49** (blue symbols); hypercrosslinked poly(vinylbenzyl chloride) (HCPVBC) "Davankov resins" (green symbols). (b) Hydrogen uptake at 1.13 bar/77.3 K as a function of the Langmuir surface area as calculated from the H_2 isotherm for the same series of hypercrosslinked polymers (samples labeled as in part a). Dashed line shows linear fit ($r^2 = 0.9927$) for the combined DCX dataset, **1**−**41**.

(40) Nijkamp, M. G.; Raaymakers, J.; van Dillen, A. J.; de Jong, K. P. *Appl. Phys. A: Mater. Sci. Process.* **2001**, *72*, 619.
(41) Rouqueol, F.; Roquerol, J.; Sing, K. *Adsorption by Powders and Porous Solids*; Academic Press: London, 1999.
(42) Aranovich, G. L.; Donohue, M. D. *J. Colloid Interface Sci.* **1997**, *189*, 101.

Langmuir assumptions.[32] Germain et al. showed recently[32] for a range of commercial polymer resins and hypercrosslinked polystyrene materials that surface areas calculated from the application of the Langmuir equation to H_2 isotherms at 77.3 K were much lower than the corresponding N_2 BET surface areas. Similarly, Zhao et al. have demonstrated linear Langmuir graphs for H_2 on activated carbon at 77.3 K in the pressure range 0.15−1 bar.[3] We have also obtained linear Langmuir graphs for **1**−**49** at 77.3 K over a similar hydrogen pressure range (see the Supporting Information, Figure S2). Figure 4b shows a plot of the maximum H_2 uptake observed (77.3 K, 1.13 bar) versus the surface area as calculated by applying the Langmuir equation to the H_2 adsorption isotherms (in the range 0.15−1.13 bar) for samples **1**−**49**. A very good linear correlation exists for all of these data, suggesting that this Langmuir surface area is a much better descriptor for the H_2 uptake capacity for these materials. Indeed, the data of Germain et al.[32] fall on a similar line (see the Supporting Information, Figure S3), shifted perhaps to reflect the slightly higher maximum H_2 pressure (1.2 bar) employed in that study. Of course, both the H_2 uptake at 1.13 bar and the Langmuir plot are derived from the same sorption datasets; as such, a correlation would be expected. It is not obvious, however, that all samples would fall on a common line in this plot unless the H_2 sorption isotherms were all of very similar shapes or all samples were at saturation (unlikely at 1.13 bar). Indeed, the plot illustrates that the HCPVBC and BCMBP samples fall slightly below the fitted regression line for the DCX materials; this is a consequence of the DCX samples adsorbing more H_2 at lower pressures due to the preponderance of ultramicropores and relative absence of supermicropores and mesopores (see discussion below). This effect is even more pronounced at lower pressures where the poly(DCX) H_2 sorption isotherms are initially steeper and then cross those measured for the HCPVBC and BCMBP materials. From the gradient of the linear fit shown in Figure 4b, it is possible to calculate an average specific H_2 capacity of 1.53×10^{-5} g H_2/m^2 for these DCX-based polymers on the basis of this Langmuir surface area. This does not represent the maximum saturation capacity for these materials but is rather the specific capacity per unit surface area under these particular conditions (1.13 bar/77.3 K). Taking that into account, the value compares well with other measures of H_2 capacity for materials such as activated carbon where 2.2×10^{-5} g H_2/m^2 was reported.[43,44] There are limitations, however, to the Langmuir model; it is most valid for absolute adsorption isotherms (as opposed to excess adsorption measurements) at relatively low pressures and at temperatures well above the critical temperature for H_2 (−240.17 °C).[44] It is therefore not reasonable to use this model to extrapolate to higher pressure behavior, particularly at a temperature of 77.3 K.[44] We therefore investigated the H_2 uptake of these materials at higher pressures (up to 15 bar) by using a gravimetric sorption analyzer (Figure 5).[9,31] Very good agreement (within experimental error) was found between sorption data obtained

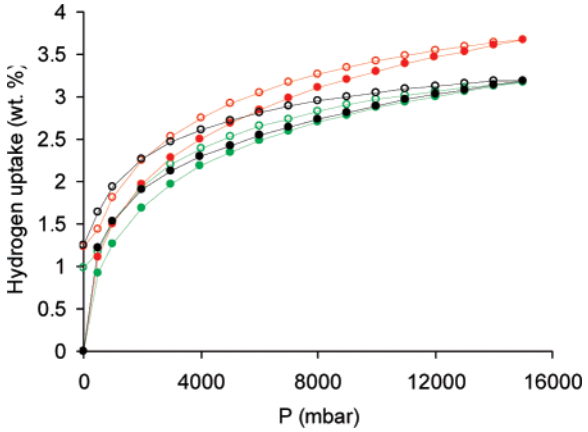

Figure 5. Gravimetric H_2 adsorption isotherms (filled symbols) and desorption isotherms (open symbols) for hypercrosslinked polymer networks up to 15 bar and 77.3 K. *p*-Dichloroxylene network (*p*-DCX), **27** (black symbols; max. uptake = 3.18 wt %); BCMBP/*p*-DCX copolymer network, **43** (red symbols; max. uptake = 3.68 wt %); hypercrosslinked poly(vinylbenzyl chloride) (HCPVBC) "Davankov resin"[31] (green symbols; BET surface area = 1657 m^2/g; max. uptake = 3.17 wt %).

using volumetric methods (Table 1) and this gravimetric technique. The maximum gravimetric H_2 uptake observed under these conditions was 3.68 wt % (**43**, Figure 5). Material **43** was derived from BCMCP and exhibited both the highest BET surface area of all the samples studied (1904 m^2/g) and the second-highest Langmuir surface area as calculated from the H_2 isotherm (1033 m^2/g). This represents the largest H_2 uptake reported so far for an amorphous organic polymer[24,31,32] and is 21% higher than the maximum uptake reported previously for our hypercrosslinked polystyrene material.[31] The H_2 sorption was found to be reversible for all materials, although there was evidence for hysteresis in the isotherms (Figure 5), especially for the *p*-DCX-based material, **27**. Previously, we tentatively ascribed this phenomenon in hypercrosslinked poly(vinylbenzyl chloride) (HCPVBC) materials to a degree of kinetic trapping in the tortuous micropore network.[31] These new data support this interpretation, because the hysteresis is greatest for samples (e.g., **27**) with the smallest average pore widths (see below).

The pore structure for **27**, **43**, and a HCPVBC sample was investigated in detail by N_2 adsorption/desorption at 77.3 K (Figure 6). All three materials showed a distinct step in the N_2 isotherm (up to approximately 200 cm^3/g STP; Figure 6, inset) at low relative pressures ($P/P_o < 0.1$) corresponding to gas sorption in micropores.[41] At higher relative pressures, however, the isotherms for the three materials differed quite markedly. The N_2 isotherm for the HCPVBC sample is very similar to that reported by us[31] and by others[32] and can be classified as Type 1B,[41] which is consistent with a material that is substantially microporous. The isotherm shows relatively little hysteresis and is broadly similar, for example, to N_2 isotherms reported for certain polymers of intrinsic microporosity (e.g., CTC-network-PIM).[24] Sorption analysis for **27** (produced from *p*-DCX) also revealed a micropore step at low P/P_o, but this isotherm exhibits greater Type II character and displays pronounced pore filling (up to ∼2000 cm^3/g) at high relative pressures, consistent with the presence of larger pores that allow unrestricted multilayer adsorption.[41] Only a small degree of hysteresis was observed upon desorption (Figure 6). The isotherm for **43** (based on

(43) Jhi, S. H.; Kwon, Y. K.; Bradley, K.; Gabriel, J. C. P. *Solid State Commun.* **2004**, *129*, 769.
(44) Benard, P.; Chahine, R. *Langmuir* **2001**, *17*, 1950.

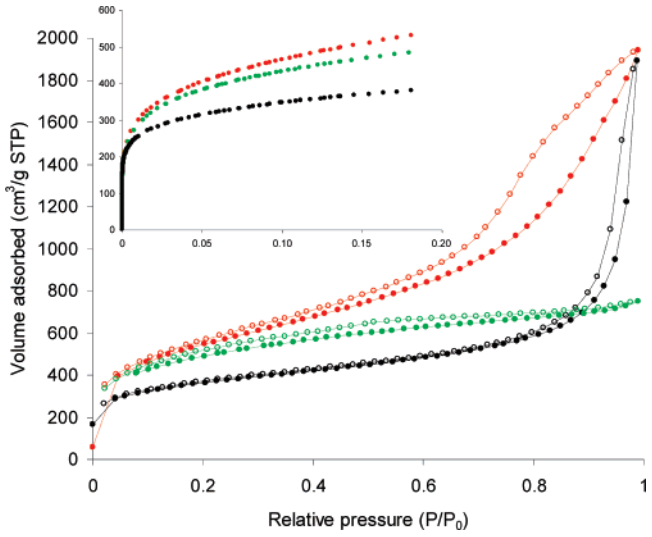

Figure 6. Nitrogen adsorption isotherm (filled symbols) and desorption isotherm (open symbols) at 77.3 K. *p*-Dichloroxylene network (*p*-DCX), **27** (black symbols); BCMBP/*p*-DCX copolymer network, **43** (red symbols); hypercrosslinked poly(vinylbenzyl chloride) (HCPVBC) "Davankov resin"[31] (green symbols). Inset shows the detail of the adsorption isotherm for the three samples in the low-pressure regime.

BCMBP) was also broadly Type II in nature but with evidence of some Type IV character. A much larger hysteresis loop was apparent at high relative pressures for this sample. The presence of larger pores and a bimodal microporous−mesoporous pore size distribution for samples **27** and **43** can be rationalized by the mode of synthesis. The microporosity in the HCPVBC sample was generated by hypercrosslinking of a solvent-swollen, single-phase, lightly crosslinked gel. It is known that phase separation does not occur in these reactions[27,28] and that the porosity formed is essentially molecular in character, that is, microporous. Application of the Barrett−Joyner−Halenda (BJH) method[45] to the isotherm for the HCPVBC material showed very little contribution from mesopores (see the Supporting Information, Figure S4). By contrast, both **27** and **43** were synthesized by condensation polymerization starting with a homogeneous solution of monomer and catalyst followed by phase separation and the precipitation of a highly porous powder. As such, **27** and **43** did not originate from a homogeneous gel phase. It is likely that microgel particles are formed in the first instance and that successive aggregation of these smaller particles leads to the porous precipitated powders obtained.[46] Mesopores (or even macropores) may arise from the interstitial voids between these primary particles.[19,46] Analysis by FE-SEM supports this hypothesis; the morphologies observed for **27** and **43** differ from that exhibited by the HCPVBC material and there is clear evidence of porosity on the >20 nm length scale for the materials that were produced by precipitation polycondensation (see the Supporting Information, Figure S5). This was confirmed by BJH analysis for **27** and **43**, which showed a distribution of mesopores and (for **27**) macropores (>50 nm; see the Supporting Information, Figure S4). This distinction between HCPVBC and samples **27** and **43** is illustrated by the

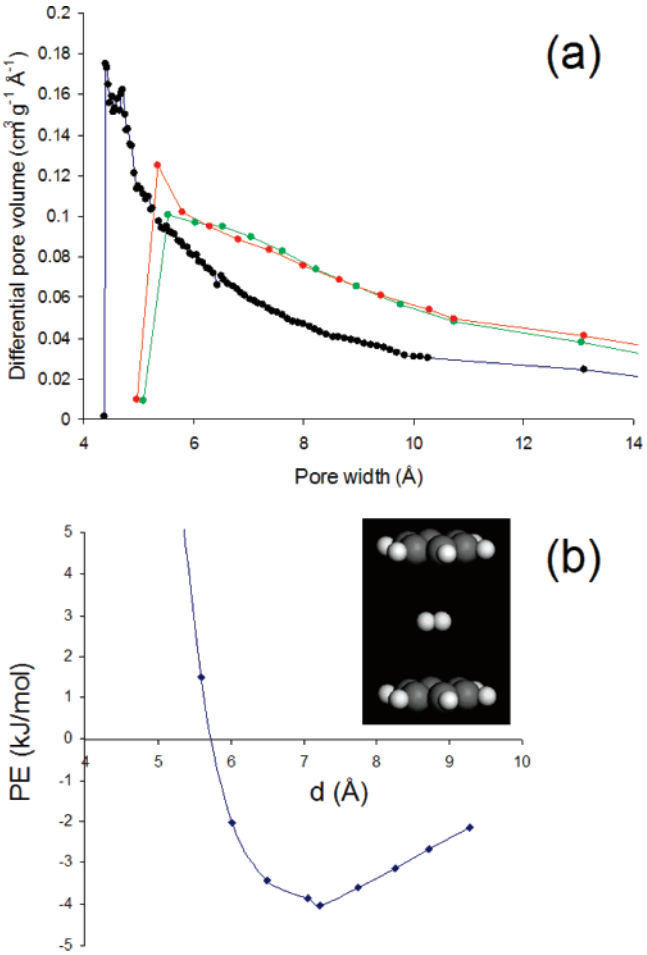

Figure 7. (a) Micropore size distributions for the polymers calculated by the Horvath−Kawazoe method (carbon slit pore model). *p*-Dichloroxylene network (*p*-DCX), **27** (black symbols); BCMBP/*p*-DCX copolymer network, **43** (red symbols); hypercrosslinked poly(vinylbenzyl chloride) (HCPVBC) "Davankov resin"[31] (green symbols). (b) Density functional theory (DFT) calculation of potential energy for dihydrogen between two parallel benzene rings as a function of the C−C spacing between the rings. Inset shows H_2 between benzene rings separated by 7.2 Å.

cumulative BJH pore volumes for pores >1.7 nm (Table 2).[47] It is unlikely that meso- and macroporosity makes a significant contribution to the H_2 uptake and such pores may therefore be detrimental to the overall volumetric storage capacity. The porous properties of **27**, **43**, and the HCPVBC material are summarized in Table 2. The sample based on BCMBP, **43**, displayed the highest H_2 uptake at 15 bar (3.68 wt %); this sample was also found to have the highest micropore volume (Table 2), whether measured from the N_2 sorption isotherm at $P/P_0 = 0.053$ (0.633 cm^3/g) or from density functional theory (DFT) calculations for pores smaller than 2 nm (0.54 cm^3/g).[48] The micropore size distributions for the three samples, as calculated using the Horvath−Kawazoe (HK) method,[24,31,49] are shown in Figure 7a. The

(45) Barrett, E. P.; Joyner, L. G.; Halenda, P. P. *J. Am. Chem. Soc.* **1951**, *73*, 373.
(46) Sherrington, D. C. *Chem. Commun.* **1998**, 2275.
(47) There is evidence for limited large micropore/small mesopore character in HCPVBC over the range 1.7−10 nm (see the Supporting Information, Figure S4), but there is no indication of pores larger than about 10 nm either by gas sorption or by FE-SEM analysis (see the Supporting Information, Figure S5).
(48) The broad trends in micropore size are similar for both methods; in particular, **27** shows an ultramicropore "spike" in the distribution centered at around 0.5 nm in both Horvath−Kawazoe and DFT slit pore analyses.
(49) Horvath, G.; Kawazoe, K. *J. Chem. Eng. Jpn.* **1983**, *16*, 470.

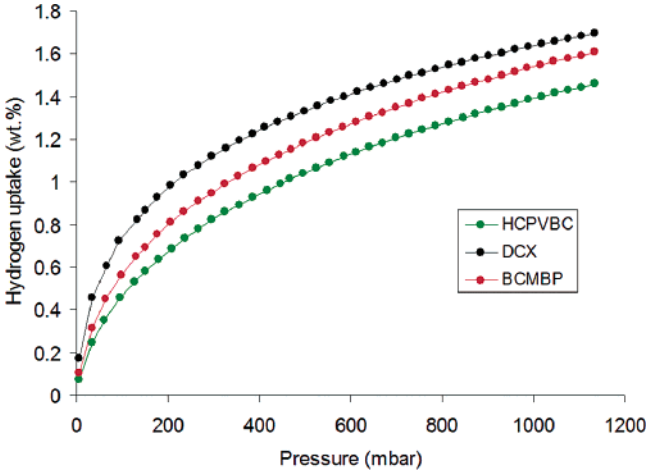

Figure 8. Volumetric H_2 adsorption isotherms up to 1.13 bar at 77.3 K. *p*-Dichloroxylene network (*p*-DCX), **27** (black symbols); BCMBP/*p*-DCX copolymer network, **43** (red symbols); hypercrosslinked poly(vinylbenzyl chloride) (HCPVBC) "Davankov resin"[31] (green symbols).

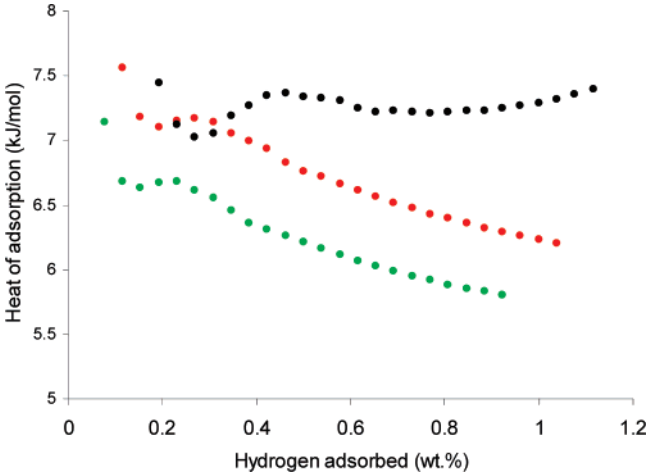

Figure 9. Isosteric heats of sorption for dihydrogen on hypercrosslinked polymers. *p*-Dichloroxylene network (*p*-DCX), **27** (black symbols); BCMBP/*p*-DCX copolymer network, **43** (red symbols); hypercrosslinked poly(vinylbenzyl chloride) (HCPVBC) "Davankov resin"[31] (green symbols).

corresponding median pore widths are listed in Table 2. All three polymers show a distribution of micropores in the range 0.4−1.4 nm when HK analysis was applied, although it should be noted that the slit pore assumptions of the HK model may be tenuous for these systems. As such, pore size distributions were also calculated using DFT methods[32] (both cylindrical and slit pore models; see the Supporitng Information, Figures S6−S8). In general, similar although not identical trends were observed using DFT treatments. The median pore widths (Table 2) for the samples were in the range 0.7−0.9, nm which is close to the optimal pore dimensions cited recently for the hydrogen sorption by copper-based MOFs[10] and for other micro- and mesoporous sorbents.[4] Interestingly, we have performed DFT calculations for dihydrogen between two parallel benzene rings (Figure 7b), which suggest that the spacing between the rings that leads to the lowest potential energy is around 0.72 nm, in broad agreement with other calculations and measurements for graphene sheets[50] and for sandwiched corannulene.[51] The micropore size distribution was not identical for the three samples; **27** (produced from *p*-DCX) had a higher proportion of ultramicropores (<0.7 nm) than HCPVBC or **43**, both as calculated by HK and DFT methods. Even though the total micropore volume for **27** is somewhat lower than for HCPVBC or **43**, the preponderance of these ultramicropores leads to enhanced H_2 uptake at lower pressures for this sample. This is evidenced by the fact that the volumetric H_2 sorption isotherm for **27** is steeper in the low-pressure range and crosses the isotherms for HCPVBC and **43** at higher relative pressures (Figure 8). The existence of these ultramicropores (which peak in the HK distribution at around 0.45 nm) is also evident in pore size distributions for **27**, as calculated by DFT methods (see the Supporting Information, Figure S6) and is manifested in a semilogarithmic plot of N_2 adsorption at very low relative pressures ($P/P_0 < 1 \times 10^{-4}$; Figure S9). These data may also suggest, however, that some of the pores in **27** are too small to allow favorable interactions with H_2 (see Figure 7b) or indeed small enough to size-exclude gases such as N_2 or even H_2 itself.

The isosteric heat of sorption for dihydrogen on these samples was calculated as a function of H_2 coverage from comparison of the adsorption isotherms at 77.3 and 87.2 K (Figure 9).[17,52] Overall, the heat of sorption was found to range between around 6 and 7.5 kJ/mol. These values are similar to those measured for a number of MOFs[17,52] and for mesoporous ordered carbons.[53] The highest average heat of sorption was observed for **27** (around 7.25 kJ/mol over this coverage range); this may reflect the preponderance of ultramicropores in this sample (median pore width = 7.384 nm) and the possibility for favorable interactions of H_2 with more than one pore wall (Figure 7b).

Atomistic Simulation of Polymer Structure and Gas Sorption. Amorphous microporous materials present a particular challenge in terms of gaining a molecular-level understanding of the nature of the pore structure and interactions of gases such as H_2 within these pores. This is because there a very few direct probes for the detailed molecular structure of these polymers. It is not possible, for example, to determine that the structure by X-ray diffraction as is done for crystalline materials such as MOFs.[7−14,17,52] Moreover, techniques such as solid-state NMR (see above) can give details regarding functionality and connectivity but can only give information on the average topologies of these complex macromolecules. We have therefore employed atomistic simulations in combination with detailed physical characterization in order to better understand these materials.

A series of models was constructed using Materials Studio Modeling 4.0 to describe the structure of polymer **27** (based on *p*-DCX). This software package has been used previously

(50) (a) Heine, T.; Zhechkov, L.; Seifert, G. *Phys. Chem. Chem. Phys.* **2004**, *6*, 980. (b) Patchkovskii, S.; Tse, J. S.; Yurchenko, S. N.; Zhechkov, L.; Heine, T.; Seifert, G. *Proc. Natl. Acad. Sci. U.S.A.* **2005**, *102*, 10439.
(51) Scanlon, L. G.; Balbuena, P. B.; Zhang, Y.; Sandi, G.; Back, C. K.; Feld, W. A.; Mack, J.; Rottmayer, M. A.; Riepenhoffl, J. L. *J. Phys. Chem. B* **2006**, *110*, 7688.
(52) (a) Dinca, M.; Yu, A. F.; Long, J. R. *J. Am. Chem. Soc.* **2006**, *128*, 8904−8913. (b) Kaye, S. S.; Long, J. R. *J. Am. Chem. Soc.* **2005**, *127*, 6506. (c) Culp, J. T.; Matranga, C.; Smith, M.; Bittner, E. W.; Bockrath, B. *J. Phys. Chem. B* **2006**, *110*, 8325.
(53) Roussel, T.; Pellenq, R. J. M.; Bienfait, M.; Vix-Guterl, C.; Gadiou, R.; Beguin, F.; Johnson, M. *Langmuir* **2006**, *22*, 4614.

Table 2. Porosity Data for Selected Hypercrosslinked Polymer Networks

	micropore volume (cm^3/g; $P/P_0 = 0.053$)[a]	micropore volume (cm^3/g; <2 nm, DFT)[b]	median pore width (nm)[c]	cumulative pore volume (cm^3/g; BJH, >1.7 nm)[a]
27	0.494	0.46	0.738	2.646
HCPVBC	0.598	0.51	0.868	0.739
43	0.633	0.54	0.888	2.798

[a] Determined from the adsorption branch of the N_2 isotherm at 77.3 K. [b] Slit pore model used in DFT calculations. [c] As calculated using the Horvath−Kawazoe method.

Table 3. Experimental and Simulated Physical Properties for *p*-DCX Network, 27

	surface area (m^2/g)	absolute density (g/cm^3)	bulk density (g/cm^3)	micropore volume (cm^3/g)	median pore width (nm)	wt % Cl	H_2 uptake (wt %)
experiment, **27**	1370[a]	1.28[b]	0.78[c] (0.42)	0.494 (0.46)[d]	0.738[e]	5.24	1.69[f]
p-DCX model[g]	2519[h]	1.23[i]	0.73[i]	0.551[i]	0.3−1.0[j]	5.50	5.37[k]
PS model[g]	833[h]	1.14[i]	1.05[i]	0.074[i]			1.23[k]

[a] Apparent surface area, five-point BET using N_2 as the sorbate at 77.3 K. [b] Measured by helium pycnometry. [c] Calculated using methods described in ref 28; figure in parentheses determined by Hg intrusion porosimetry. [d] Determined from the N_2 at isotherm at $P/P_0 = 0.053$; figure in parentheses determined by slit-pore DFT calculation. [e] Calculated using the Horvath−Kawazoe method. [f] Measured volumetrically at 77.3 K and 1.13 bar. [g] All properties calculated using Materials Studio 4.0. [h] Connolly surface area; probe radius = 1.82 Å. [i] Calculated using the occupied and unoccupied volumes in the amorphous simulation cell. [j] Estimated from slices of the simulated pore structure, Figure 10c. [k] Calculated using the Sorption module in Materials Studio 4.0 (1.13 bar, 77.3 K).

to model H_2 adsorption/desorption in magnesium[54] and in zeolites,[55] as well as gas permeation through microporous membranes,[56] to elucidate the structure of intercalated silicates,[57] and ion exchange in zeolite beta.[58] The models were built in several stages; first, a repeating unit for the polymer was defined. Solid-state NMR for *p*-DCX-based polymers (see above) showed that, on average, each aromatic group bears approximately three substituents. To achieve this ratio, we constructed a dimer of *p*-DCX as based on the repeat unit shown in Figure 3a. As outlined above, this is likely to be an overly simplistic view of the bonding in these materials but the approach facilitates the iterative building of a range of structures. The *p*-DCX dimer was combined using the Polymer Building tool in Materials Studio to create clusters of poly(*p*-DCX) covering a range of molecular weights. All of these models were fully relaxed using the Discover molecular mechanics and dynamics simulation module using the COMPASS forcefield.[36] The Amorphous Cell module was then used to combine these relaxed clusters in various ratios to produce a range of amorphous simulation cells, each of which had periodic boundary conditions and can be considered as a unit in an infinite three-dimensional lattice. Two additional characterization methods were used to help construct the models. First, elemental analysis for **27** showed the composition to be C, 81.96; H, 5.38; Cl, 5.24. As such, the target for residual unreacted chloromethyl groups in the model was set to achieve ∼5 wt % chlorine loading. A second important input parameter was the "target" bulk density for the model because this defines, to a large degree, the pore volume in the resulting simulation. The skeletal density of **27** was measured by mercury porosimetry to be 0.42 g/cm^3. Because mercury porosimetry does not measure pores smaller than about 7 nm,[19] this can be considered to be a measure of the bulk density for the polymer, including contributions from any Hg-inaccessible mesopores or occluded porosity.[59] An alternative estimate of the bulk density of the microporous polymer domains (excluding the effects of any mesoporosity) can be gained from the relationship $W_0 = 1/\rho_{app} - 1/\rho_{tr}$, where W_0 is the specific pore volume, ρ_{app} is the apparent (or bulk) density, and ρ_{tr} is the true (or absolute) density.[28] If W_0 is assumed to be the micropore volume (0.494 cm^3/g) and the absolute density, ρ_{tr}, is 1.28 g/cm^3, then the bulk density of the microporous domains can be calculated to be 0.78 g/cm^3. We consider this latter figure to be more reasonable as a "target" bulk density for the simulations,[59] and the value agrees well with the measured bulk densities for a series of exclusively microporous hypercrosslinked polystyrenes, which fall in the range 0.71−0.91 g/cm^3.[28]

A model was selected from a number of candidates that gave the best overall agreement with the characterization data for the physical sample (Table 3). This particular model was constructed from a combination of poly(*p*-DCX) clusters containing 500 carbon atoms and 60 carbon atoms, respectively, in a 2:3 ratio. The model was again fully relaxed using the Discover module and the COMPASS[36] forcefield to ensure that the cell parameters and hence the density remained constant. A Connolly surface[60] was created for the model using the Atom, Volumes and Surface module in Materials Studio using a coarse grid resolution and a Connolly radius set to 1.82 Å (the kinetic radius of N_2).

(54) Liang, J. J. *Appl. Phys. A: Mater. Sci. Process.* **2005**, *80*, 173.
(55) Vitillo, J. G.; Ricchiardi, G.; Spoto, G.; Zecchina, A. *Phys. Chem. Chem. Phys.* **2005**, *7*, 3948.
(56) Yin, K. L.; Xu, D. J. *Chem. Eng. Commun.* **2006**, *193*, 1678.
(57) Capkova, P.; Pospisil, M.; Weiss, Z. *J. Mol. Model.* **2003**, *9*, 195.
(58) Sun, P. P.; Deore, S.; Navrotsky, A. *Microporous Mesoporous Mater.* **2006**, *91*, 15.

(59) These DCX-based materials are not exclusively microporous but contain pores in the range 2−7 nm (see Figure 7a and the Supporting Information, Figure S4) that would be inaccessible to Hg porosimetry and will therefore lower the skeletal density as measured by this technique, even if perfect pore connectivity and a lack of any occluded porosity is assumed (the latter would reduce the measured density still further). As such, this measured density of 0.42 g/cm^3 reflects the nature of the mesostructured sample but represents a significant underestimate for our atomistic simulations which deal only with the microporous domains. In practice, it proved very difficult to construct chemically plausible models with simulated bulk densities of less than about 0.5−0.6 g/cm^3; this supports the notion that the low porosimetry value stems from mesoporosity.

(60) Connolly, M. L. *Science* **1983**, *221*, 709.

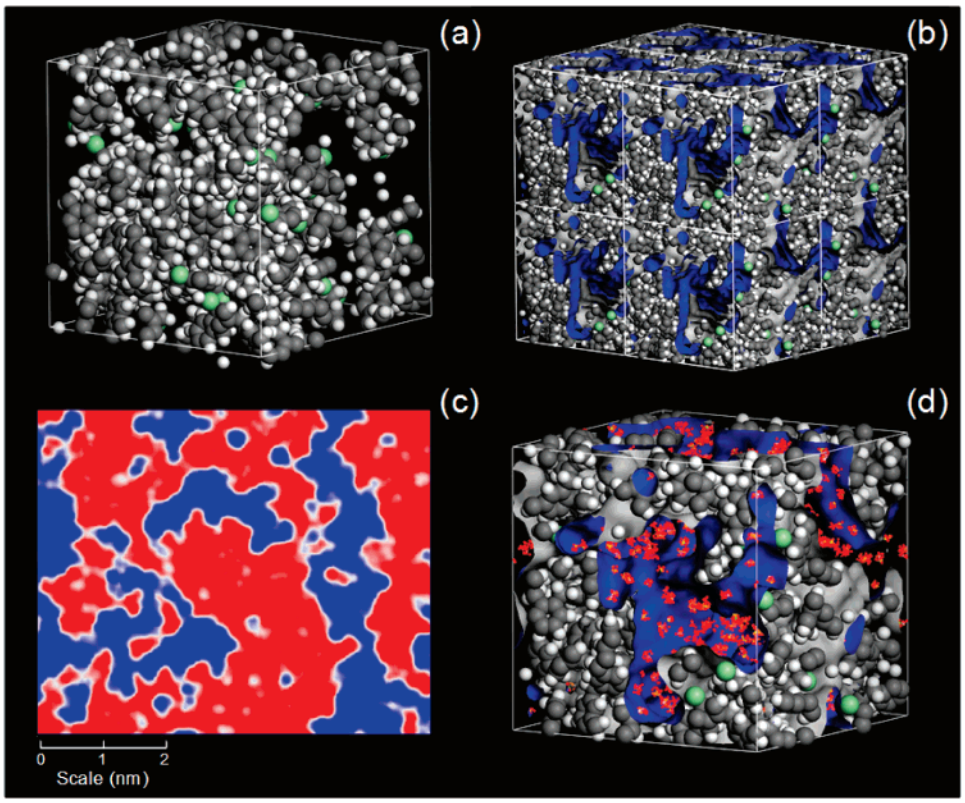

Figure 10. (a−c) Molecular simulation of *p*-DCX network and (d) H_2 sorption properties. (a) Simulated poly(*p*-DCX) network, Connolly surface area = 2519 m^2/g, simulated micropore volume = 0.551 cm^3/g. Dimension of simulation box (the "amorphous cell") = 3.3175 nm (also see the Supporting Information, Figure S11). (b) Three-dimensional array of eight amorphous cells with periodic boundary conditions. A Connolly surface is shown in blue/gray. (c) Two-dimensional "slice" through an array of amorphous cells in the simulated pore structure. The occupied and unoccupied volumes are shown in red and blue, respectively (also see slices in 3D, the Supporting Information, Figure S15). (d) Snapshot of H_2 sorption in the simulated pore structure at 1.1 bar/77 K. The density field of the adsorbed H_2 molecules is shown in red/orange (also see density map, the Supporting Information, Figure S17).

The physical characteristics of the polymer, both measured and simulated, are summarized in Table 3. In general, the model predicts the absolute density, the bulk density, and the micropore volume relatively well. The model slightly underestimates the absolute and bulk densities and overestimates the micropore volume. This can be explained to some degree by the fact that the simulation ascribes surface area and pore volume to areas within the cell that are clearly occluded and not connected to the rest of the pore structure (see the Supporting Information, Figure S10). Such occluded free volume would reasonably be expected to occur within these polymers[22,27,28] but would not be accessible to sorbate gases such as N_2, H_2, or even He in gas sorption and pycnometry measurements. The Connolly surface area (2519 m^2/g) was found to be much greater than the experimental BET value (1370 m^2/g) but closer to the Langmuir surface area (2096 m^2/g). Similar comparisons have been made for MOF samples where the Connolly surface area has also been shown to be double the measured BET surface area in some cases.[17] The overestimation of surface area and pore volume was also rationalized by constructing a model for atactic polystyrene (bulk density 1.05 g/cm^3), which is in reality nonporous and has no permanent interconnected pore structure.[61] A Connolly surface area of 833 m^2/g and a pore volume of 0.074 cm^3/g were calculated from the simulation. This clearly results from occluded free volume rather than interconnected micropores (see the Supporting Information, Figure S11).

Figure 10 shows a series of visualizations generated from the poly(*p*-DCX) model. A space-filling representation of the amorphous cell is shown in Figure 10a (see the Supporting Information, Figure S13 for expanded figure with Connolly surface). A 2 × 2 × 2 array of amorphous cells is shown in Figure 10b. This illustrates how an interconnected micropore structure can be simulated by packing these amorphous cells with periodic boundary conditions. Figure 10c shows a two-dimensional "slice" through the simulated pore structure (the unoccupied pore volume is colored blue). The model simulates the pore micropore dimensions quite well; the majority of the pore channels are between 0.3 and 2.0 nm in width. Figure 10c demonstrates the presence of pockets of occluded volume (also see the Supporting Information, Figures S10 and S15) as well as interconnected micropores. As mentioned above, this model simulates only microporosity in the material and does not account for meso- or macroporosity; indeed, N_2 sorption analysis shows (see the Supporting Information, Figure S4) that there are mesopores in **27** with widths that are larger than the dimensions of the simulation cell (3.318 nm).

Hydrogen sorption isotherms were calculated at 77.3 and 87.2 K for this model using the Sorption module within

(61) The polystyrene model was constructed from atactic chains of 20 repeat units. The amorphous cell was built with 10 chains per unit cell packed to a target density of 1.05 g/cm^3 (the bulk density of amorphous polystyrene).

Materials Studio. The Universal forcefield was used at a medium-quality calculation level. Figure 10d shows a visualization of the H_2 sorption in the material at 1.1 bar and 77.3 K (the average positions of the H_2 molecules are shown in orange/red). The sorption simulation predicts a total H_2 uptake of 5.4 wt % at 1.1 bar, much higher than the experimentally determined value for **27** of 1.69 wt %. This can be explained, at least in part, by the over-prediction of surface area and the simulated sorption of H_2 in areas of occluded volume that would not be accessible in the actual polymer (see the Supporting Information, Figure S10). Indeed, nonporous atactic polystyrene was modeled to have a H_2 uptake of 1.23 wt % under these conditions (Table 3; the Supporting Information, Figure S11) when in reality, the degree of sorption would be expected to be negligible. Surblé et al.[11] have recently modeled the H_2 sorption properties of MIL-102, a chromium carboxylate MOF, and found a very good fit with the experimental isotherm when a scaling factor, Φ, of 0.76 was applied to take into account inaccessible pores and nonporous defects. As such, Φ represents the ratio of the experimental to the theoretical pore volume.[11] In our simulation, it is also possible to fit the shape of the sorption isotherms (Figure 11a) at both 77.3 and 87.2 K, but more dramatic scaling factors are required ($\Phi_{77K} = 0.305$; $\Phi_{87K} = 0.285$). One contribution to this low Φ value is the significant degree of "false sorption" in occluded pores in the simulation, as mentioned above. It is also possible that larger tracts of micropore volume may be disconnected and occluded in the physical sample, including pores with lengths that exceed the dimensions of the amorphous cell employed here. We believe that it is the overestimation of pore connectivity and accessibility (arising in part from the relatively small simulation box and periodic boundary conditions) that accounts for the artificially high sorption in this model, rather than, for example, a gross misrepresentation of the pore size distribution (cf. Figures 7a and 10c). When scaled, the shape of the simulated isotherms agrees very well with the experimental data at both 77.3 and 87.2 K (Figure 11a). In keeping with this, the simulation predicts the sorption enthalpy quite well (Figure 11b). The peak in the simulated distribution of H_2−polymer interaction energies is centered around 7.5 kJ/mol in comparison with a measured isosteric heat of adsorption for **27** of between 7 and 7.5 kJ/mol (Figure 9). The simulation does not predict any high-energy binding sites (−15 kJ/mol or greater), which is consistent[15] with the fact that these polymers exhibit negligible H_2 uptake at ambient temperature, at least up to 1.13 bar. It should be noted that the value used for the scaling factor, Φ, of approximately 0.3 was an arbitrary figure that was chosen to give the best fit between the experimental and simulated isotherms. This Φ value is significantly lower than the ratio of the experimental and simulated micropore volumes (0.89) or the ratio of the N_2 BET surface area and the modeled Connolly surface area (0.55). The value of Φ is closer to the ratio of the Langmuir surface area (as calculated from the H_2 isotherm) and the modeled Connolly surface area (0.39); again, this is consistent with a significant overestimation of physical surface area in the samples that arises from the application of the BET model.

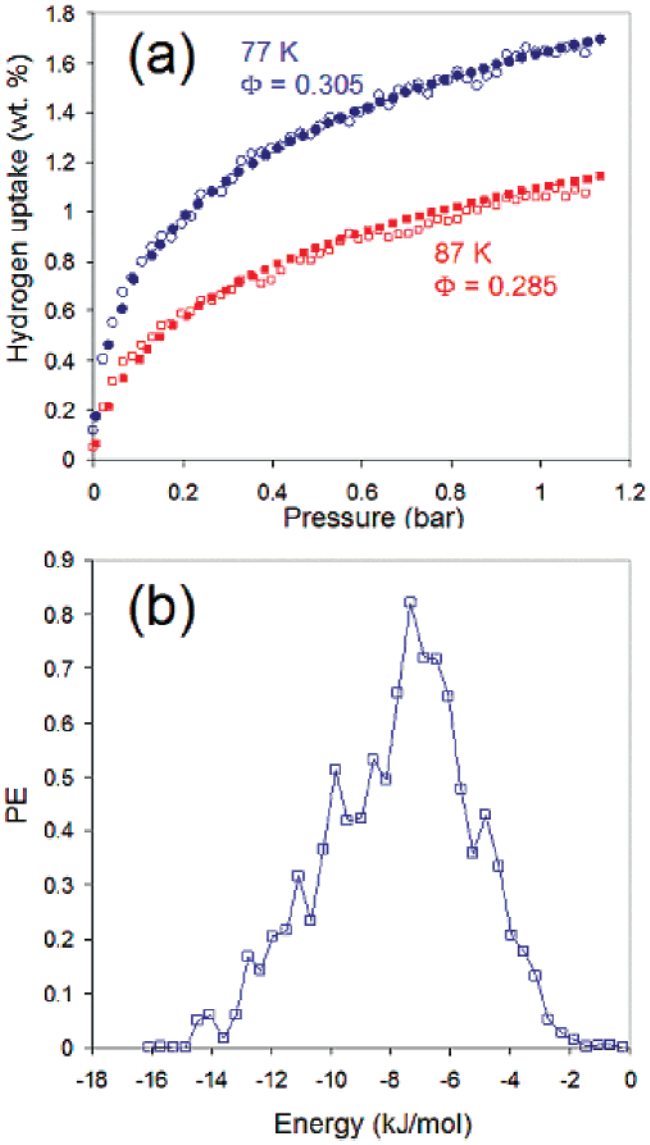

Figure 11. (a) Measured (closed circles) and simulated (open circles) H_2 sorption isotherms at 77 K (blue) and 87 K (red). A scaling factor, Φ, has been applied to the simulated data in each case. (b) Simulated distribution of H_2 sorption energies in the polymer network (77.3 K, 1.1 bar). The *y*-axis represents a distribution function, PE, which is a measure of the probability of a sorbate molecule being at a given sorption energy.

Discussion

This study provides a number of important insights into both the design of microporous organic polymers and the optimization of H_2 uptake in such materials. Hypercrosslinked polystyrene materials have been known for some time[27,28] and even commercialized in some formats[32] but the unusual properties of these materials (permanent microporosity, detailed molecular structure, significant swellability in thermodynamically bad solvents for the polymer network) are only partially understood. In particular, the molecular nature of the porosity in such materials has been difficult to study directly; solid-state NMR[37] has provided detailed information regarding the bonding in such polymers, but this is not readily translated into a 3-dimensional structural model. ^{129}Xe NMR was employed to study hypercrosslinked pol-

yarylcarbinols,[62] and two potential models were proposed to account for the swelling behavior of these materials. Model 1 (supported by the NMR evidence) assumed highly crosslinked microgel particles connected by flexible linkers, whereas Model 2 assumed a more homogeneous morphology.[62] Our atomistic simulations show clearly that it is difficult to construct a "homogeneous" model that gives rise to pores in the 0.5−1 nm range. By contrast, a network of chemically linked microgel particles (Model 1) can explain quite well the physical characteristics of these polymers. This study also shows, for the first time, that materials synthesized by the polycondensation of bischloromethyl monomers may have some advantages (both in terms of synthetic versatility and absolute surface areas) over more standard "Davankov-type" resins.[27,28,30,37] It is also clear that the polycondensation route produces mesostructure as a result of a heterogeneous aggregation process; this may be a strong advantage for some applications (hierarchical porosity, improved mass transport) but a potential disadvantage in others (e.g., reduced volumetric gas storage capacity). The majority of hypercrosslinked polymers have been synthesized from a limited range of monomers such as styrene[27,28] and vinylbenzyl chloride.[30] We show here that just small changes to the monomer structure can have a dramatic influence on the microporosity of the polymers − the rigid biphenyl monomer, BCMBP, produced materials with significantly higher BET surface areas and H_2 uptakes than any of the DCX-based polymers.

In terms of absolute gravimetric H_2 uptake, these new hypercrosslinked polymers significantly outperform other organic polymers reported thus far[23,24,31,32] at pressures of 10 bar or more but fall short of the highest uptakes reported for MOFs[8,10,13] and certain very high surface area activated carbons.[63] Our leading material (**43**) shows a gravimetric H_2 uptake (3.68 wt %) at 77.3 K and 15 bar;[64] this is broadly comparable with, for example, Al(OH)bdc (3.8 wt %)[14] IRMOF-6 (∼4.2 wt %),[8] and Cu_2L^1 (∼3.9 wt %)[10] but significantly lower than MOF-177 (∼5.5 wt %)[8] or Cu_2L^2 (∼5.75 wt %).[10] Our simulations suggest that there may be substantial "unrealized" micropore volume in these polymers, and we are currently evaluating methods to maximize pore connectivity. One potential strategy (based on the comparison between *p*-DCX and BCMBP) is to synthesize more extended bichloromethyl monomers based, for example, on terphenyl or quaterphenyl moieties. Such approaches, coupled with the fact that these materials are comprised solely of light elements, could significantly enhance the gravimetric H_2 uptake in these materials.

A more challenging problem is presented by the relatively low heats of sorption exhibited by the polymers (6−7.5 kJ/mol). Although somewhat higher enthalpies have been observed for certain MOFs[12] and carbons, a generic limitation associated with physisorptive H_2 storage is the very low-temperature that is required and the associated system weight implications. The current absence of materials that exhibit much higher isosteric heats (more than −10 kJ/mol) over a broad range of H_2 coverage severely limits the applicability of such technologies,[15] and researchers have investigated, for example, "spillover" mechanisms as one potential solution.[16] We are currently extending our simulation approaches to encompass molecular modeling of interactions of dihydrogen with a range of organic functionalities using MP2 methodologies. Our aim is to design high-energy sorption sites that might subsequently be incorporated into polymer networks of the type described here. The design of such functionality is a very challenging goal, although the synthetic versatility of organic polymer chemistry and the robustness of these networks to a wide range of reaction conditions both augur well for the inclusion of potential "binding units".

Conclusions and Outlook

There are, at present, very few synthetic routes that exist to produce microporous organic polymers with high surface areas (>1000 m^2/g) composed solely of light elements.[21,28,65] We demonstrate here that the self-condensation of bischloromethyl monomers such as DCX and BCMBP can lead to materials with enhanced gas storage properties. We have demonstrated that the porosity in these polymers is controlled not only by the level of cross-linking but also by subtle changes in the design of the rigid monomer unit, much as observed for MOFs. As such, we believe that careful design of monomer geometry has equal importance for these amorphous systems. Moreover, we have shown for the first time that atomistic simulation is a useful tool that can aid the understanding of the structure and gas sorption properties for amorphous microporous materials. A number of other linking chemistries might be considered in the future in addition to Friedel−Crafts coupling provided that the networks are designed to have sufficient rigidity to allow for permanent microporosity. It is interesting to speculate as to whether amorphous, disordered systems of this type can ultimately compete in terms of surface area and pore volume with highly ordered structures such as MOFs. It is certainly the case that the pore size distribution in these organic polymer networks is more statistical in nature. This does not mean, however, that systems cannot be designed to have micropore size distributions that are sufficiently narrow for applications such as gas storage. Our measurements and simulations suggest that there is unutilized micropore volume in the polymer networks and the maximization of pore connectivity is an important future target. If this is achieved, then we believe amorphous microporous polymers are synthetically versatile systems that can compete with ordered structures in terms of "atom efficiency" in creating micropore volume. Additional practical advantages are robustness and scalability; these materials have good thermal stability, excellent chemical robustness (e.g., to

(62) Urban, C.; McCord, E. F.; Webster, O. W.; Abrams, L.; Long, H. W.; Gaede, H.; Tang, P.; Pines, A. *Chem. Mater.* **1995**, *7*, 1325.
(63) Texier-Mandoki, N.; Dentzer, J.; Piquero, T.; Saadallah, S.; David, P.; Vix-Guterl, C. *Carbon* **2004**, *42*, 2744.
(64) We have not characterized the H_2 uptake for our materials at pressures greater than 15 bar, although we extrapolate from our sorption data that the excess gravimetric H_2 uptake for **43** at a pressure of 50 bar might fall in the range 4.0−4.5 wt % at 77.3 K.
(65) Cote, A. P.; Benin, A. I.; Ockwig, N. W.; O'Keeffe, M.; Matzger, A. J.; Yaghi, O. M. *Science* **2005**, *310*, 1166.

strong acids and bases), and are quite readily produced on a large scale.

Acknowledgment. We thank EPSRC (EP/C511794/1) and the Royal Society for a Royal Society Research Fellowship (to A.I.C.) and a Wolfson Merit Award (to M.J.R.). We thank the Centre for Materials Discovery for facilities and support.

Supporting Information Available: Langmuir plots (H_2 isotherms), BJH pore size distributions, DFT pore size distributions, electron micrographs, and expanded images of simulations. This material is available free of charge via the Internet at http://pubs.acs.org.

CM070356A